THE JOURNAL OF BIOLOGICAL CHEMISTRY
Vol. 275, No. 6, Issue of February 11, pp. 4225–4229, 2000

Printed in U.S.A.

Structure of the *Influenza* C Virus CM2 Protein Transmembrane Domain Obtained by Site-specific Infrared Dichroism and Global Molecular Dynamics Searching*

(Received for publication, September 7, 1999, and in revised form, October 22, 1999)

Andreas Kukol and Isaiah T. Arkin‡

From the Cambridge Center for Molecular Recognition, Department of Biochemistry, University of Cambridge, 80 Tennis Court Road, Cambridge CB2 1GA, United Kingdom

The 115-residue protein CM2 from *Influenza* C virus has been recently characterized as a tetrameric integral membrane glycoprotein. Infrared spectroscopy and site-directed infrared dichroism were utilized here to determine its transmembrane structure. The transmembrane domain of CM2 is α-helical, and the helices are tilted by $\beta = (14.6 \pm 3.0)°$ from the membrane normal. The rotational pitch angle about the helix axis ω for the 1-^{13}C-labeled residues Gly^{59} and Leu^{66} is $\omega = (218 \pm 17)°$, where ω is defined as zero for a residue pointing in the direction of the helix tilt. A detailed structure was obtained from a global molecular dynamics search utilizing the orientational data as an energy refinement term. The structure consists of a left-handed coiled-coil with a helix crossing angle of $\Omega = 16°$. The putative transmembrane pore is occluded by the residue Met^{65}. In addition hydrogen/deuterium exchange experiments show that the core is not accessible to water.

The virus *Influenza* is known from the past till today as the causative agent of the most deadly disease outbreaks. Recently, the CM2 protein of *Influenza* C virus (1) has been characterized as an integral membrane glycoprotein that forms disulfide linked dimers and tetramers. Based on the overall topology containing a 23-residue extracellular part, a 23-residue membrane spanning part, and a 69-residue cytoplasmic tail, CM2 is assumed to be structurally similar to the *Influenza* A M2 protein and the *Influenza* B NB protein (2, 3). The transmembrane domains of M2 and NB both form ion channels in lipid membranes (4, 5), and the M2 H^+ channel is blocked by the anti-*Influenza* drug amantadine. Because these small viral membrane proteins form possible targets for drugs, structural data may facilitate the development of new antiviral drugs.

Because of the lack of high resolution x-ray data, molecular modeling is commonly used to obtain structural models of transmembrane proteins (6, 7). The M2 transmembrane domain has been a popular choice for molecular modeling efforts (8, 9). We have applied the recently developed method of site-directed infrared dichroism (10) to the M2 transmembrane domain resulting in orientational data (11), which is in accordance with results obtained using solid state NMR (12). Further, the orientational data were used in a global molecular dynamics search to obtain a detailed structure that is in agreement with all functional and mutagenesis data (11).

Here we present the first structural data about the CM2 transmembrane domain. Initially, we characterized its secondary structure by infrared spectroscopy and showed that it is mostly α-helical. Subsequently, the approach of site-directed infrared dichroism and molecular modeling was used to determine the helix tilt, the relative orientation of the helix within the helix bundle, and a detailed structure based on this orientation.

MATERIALS AND METHODS

Peptide Purification and Reconstitution—Synthetic peptides corresponding to the predicted transmembrane domain of the *Influenza* C/Ann Arbor/1/150 virus CM2 sequence were made by solid-phase Fmoc (*N*-(9-fluorenyl)methoxycarbonyl) chemistry, cleaved from the resin with trifluoroacetic acid, and lyophilized. The sequences corresponding to residues 47–76 (numbering includes a 24 residue signal peptide) are (2) ENQGYMLTLASL([1-^{13}C]G)LGIITM([1-^{13}C]L)YLLVKIIIE and ENQGYMLTLASLGL([1-^{13}C]G)IITMLY([1-^{13}C]L)LVKIIIE, each with two carbonyl ^{13}C amino acids (Cambridge Isotopes Laboratories, Andover, MA) at positions Gly^{59} and Leu^{66} and at positions Gly^{61} and Leu^{68}, respectively. The peptides were further purified as described elsewhere (11) for analogous transmembrane peptides. Briefly, the peptide was dissolved in trifluoroacetic acid and purified by reversed phase high pressure liquid chromatography (Jupiter 5C4-300 Å column, Phenomenex, Cheshire, United Kingdom). Peptide elution was achieved with a linear gradient to a final solvent composition of 5% H_2O, 20% trifluoroethanol, 28% acetonitrile, and 47% 2-propanol (Biocad Sprint, Perceptive Biosystems, Cambridge, MA). All solvents contained 0.1% (v/v) trifluoroacetic acid. After lyophilization of pooled fractions, the peptide was reconstituted into lipid vesicles by dialysis from a solution of 5% (w/v) β-octylglycopyranoside (Melford Laboratories, Ipswich, UK) and 12.5 mg/ml dimyristoylphosphocholine (Sigma) against 0.1 mM phosphate buffer, pH 7 (11).

Infrared Spectroscopy—Fourier transform infrared (FTIR)[1] spectra were recorded on a Nicolet Magna 560 spectrometer (Nicolet, Madison, WI) equipped with a high sensitivity liquid nitrogen-cooled MCT/A detector. Attenuated total reflection-FTIR spectra were measured with a 25 reflections attenuated total reflection accessory from Graseby Specac (Kent, UK) and a wire grid polarizer (0.25 μM, Graseby Specac). 200 μl of sample (~2.5 mg/ml protein and 12.5 mg/ml lipid) were dried onto a germanium trapezoidal internal reflection element (50 × 2 × 20 mm) under a stream of nitrogen. After extensively purging the instrument with dry nitrogen, 1000 interferograms were averaged for every sample and processed with 1 point zero filling Happ-Genzel apodization. Transmission spectra were obtained by drying 50 μl of sample on a CaF_2 window with a 15-mm diameter.

Fourier self-deconvolution (13) was applied to the spectra in the amide I region to separate the overlapping ^{12}C and isotope-shifted ^{13}C (14) amide I peaks. The enhancement factor used in Fourier self-deconvolution was 2.0, and the half-height bandwidth was 13 cm^{-1}, as reported previously (15). The dichroic ratio, R, was calculated as the ratio between the integrated absorption of parallel and perpendicular polarized light of the absorption bands (between 1670 and 1645 cm^{-1} for the helix, ^{12}C, and 1610 and 1630 cm^{-1} for the site-specific label, ^{13}C. The site-specific dichroic ratio, R_{site}, was corrected for the 1.1% natural abundance ^{13}C as described (11). D_2O exchange was performed by

* This work was supported by the Wellcome Trust and BBSRC. The costs of publication of this article were defrayed in part by the payment of page charges. This article must therefore be hereby marked "*advertisement*" in accordance with 18 U.S.C. Section 1734 solely to indicate this fact.

‡ To whom correspondence should be addressed. Tel.: 44 1223 766 048; Fax: 44 1223 766 002; E-mail: sa232@cam.ac.uk.

[1] The abbreviation used is: FTIR, Fourier transform infrared.

incubating the sample for 2 h in 99% D_2O before drying. To monitor the D_2O exchange, the amide II band between 1525 and 1570 cm^{-1} was integrated, and its area A_{II} was divided by the total amide I area ($y = A_{II}/A_I$) to account for differences in protein concentration. The amount of D_2O exchange was then calculated by dividing the corrected amide II area in D_2O (y_{D_2O}) by the corrected amide II area in H_2O (y_{H_2O}).

Data Analysis—The data were analyzed according to the theory of site-specific dichroism presented in detail elsewhere (10) with the extensions described (11). Briefly, the measured dichroic ratio, the absorption ratio between parallel and perpendicular polarized light $R = A_\parallel/A_\perp$ of a particular transition dipole moment is a function of its spatial orientation. For the amide I mode (mainly the C═O bond vibration) of an α-helical protein the geometric relation between the transition dipole moment and the helix is known from fiber diffraction studies (16). Therefore, by measuring the orientation of the amide I transition dipole one can determine the helix tilt angle β and the rotational pitch angle ω of the specific dipole moment about the helix axis. The rotational pitch angle ω is arbitrarily defined as 0° when the transition dipole moment, the helix director, and the z axis all reside in a single plane. Thus, measuring the site-specific dichroic ratio R_{site} of the ^{13}C amide I mode from a particular label and the helix dichroic ratio R_{helix} allows calculation of the helix tilt β and the rotational pitch angle ω of a particular label as detailed previously (10), if measurements from two samples with labels at different ω are analyzed together. Note that the difference of ω between two consecutive residues is assumed to be 100° as in a canonical α-helix (17). To enhance the ^{13}C amide I mode intensity we introduced two labels at position i and i + 7 assuming that they posses the same ω as described elsewhere (18).

Molecular Modeling—A global search with respect to rotation about the helix axis, assuming tetrameric symmetry, was carried out as described elsewhere in detail (11, 19). In brief, all calculations were performed with the parallel processing version of the Crystallography and NMR System (Version 0.3) (20) using the OPLS parameter set with a united atom topology that explicitly represents the polar hydrogen and aromatic side chain atoms (21). All calculations were carried out *in vacuo* with the initial coordinates of a canonical α-helix (3.6 residues/turn). Symmetric tetramers were generated from the sequence YMLTLASLGLGIITMLYLLV, acetylated at the N terminus, and methylaminated at the C terminus by replicating the helix and rotating it by 360°/4 around the center of the tetramer. An initial crossing angle of 25° for left-handed and −25° for right-handed structures was introduced by rotating the long helix axis with respect to the long bundle axis. The symmetric search was carried out by applying a rotation to all helices simultaneously between $\phi = 0°$ and $\phi = 360°$ in 10° steps. Four trials were carried out for each starting structure, using different initial random atom velocities in each case at both right- and left-handed crossing angles yielding 36 × 4 × 2 equaling 288 structures. Each structure was subjected to a simulated annealing and energy minimization protocol. Clusters of similar structures were defined such that the root mean square deviation of the coordinates between all structures within a cluster was not larger than 1.2 Å; a cluster was formed by a minimum of 12 structures. For each cluster an average structure was calculated, energy was minimized, and then the structure was subjected to the same simulated annealing protocol used in the systematic search.

Orientation Refinement—To take into account the results obtained

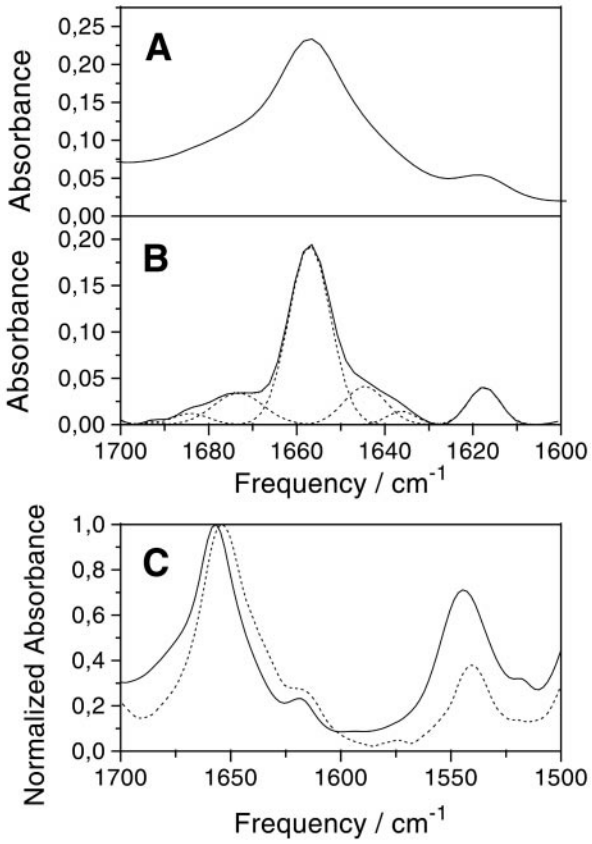

FIG. 1. **Transmission FTIR spectra of the lipid vesicle reconstituted CM2 peptide ^{13}C labeled at Gly^{59}/Leu^{66}.** The amide I region (*A*) and the same region after Fourier-self deconvolution (*B*) show the decomposition of the absorption bands into their components (*dotted lines*) obtained by fitting Gaussian curves to the spectrum. The component of the ^{13}C amide band centered at 1617 cm^{-1} is not visible because it is overlaid by the spectrum. The curvefit of the summed components is identical to the spectrum. *C,* amide I and amide II regions before (*solid line*) and after a 4-h incubation in D_2O (*dotted line*). The absorbance is normalized to the integrated area of the amide I peak centered at 1658 cm^{-1}.

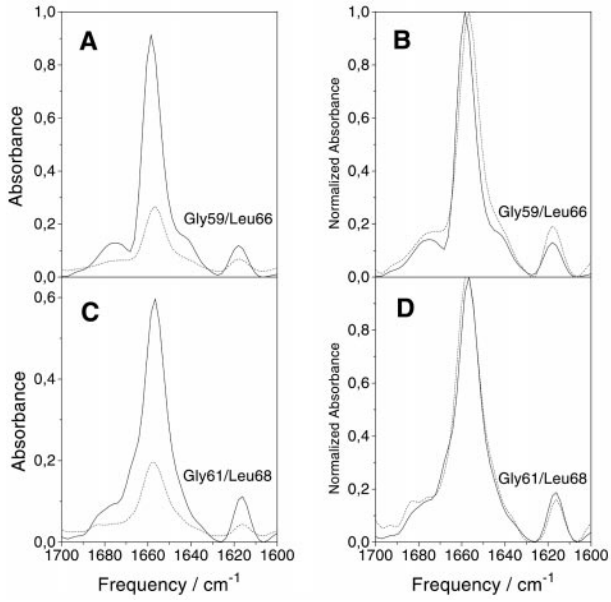

FIG. 2. **Attenuated total reflection deconvoluted FTIR spectra of the lipid vesicle reconstituted CM2 peptide ^{13}C labeled at Gly^{59}/Leu^{66} (*A* and *B*) or Gly^{61}/Leu^{68} (*C* and *D*) obtained with parallel (*solid line*) or perpendicular (*dotted line*) polarized light.** In *B* and *D* the spectra of *A* and *C* are shown whereby the absorbance is normalized to the amide I maximal intensity to show the dichroism of the ^{13}C amide I absorption band.

TABLE I
Measured dichroic ratios

Dichroic ratios for the helix R_{helix}, the ^{13}C-labeled site R_{site}, and lipid asymmetric stretching (CH_2) modes R_{lipid} for the two CM2 peptides. Also shown are the calculated lipid order parameters $S_{lipid} = (3\cos^2\beta - 1)/2$ (24), the helix tilt angle β, and the rotational pitch angle ω about the helix axis.

Peptide	R_{helix}	S_{helix}	R_{site}	R_{lipid}	S_{lipid}	β	ω
Gly^{59}/Leu^{66}	3.14 ± 0.15	0.61 ± 0.06	2.27 ± 0.12	1.18 ± 0.13	0.63 ± 0.13	14.6 ° ± 3.0 °	218 ° ± 17 °
Gly^{61}/Leu^{68}	2.83 ± 0.35	0.48 ± 0.15	3.40 ± 0.67	1.13 ± 0.04	0.68 ± 0.05	14.6 ° ± 3.0 °	58 ° ± 17 °

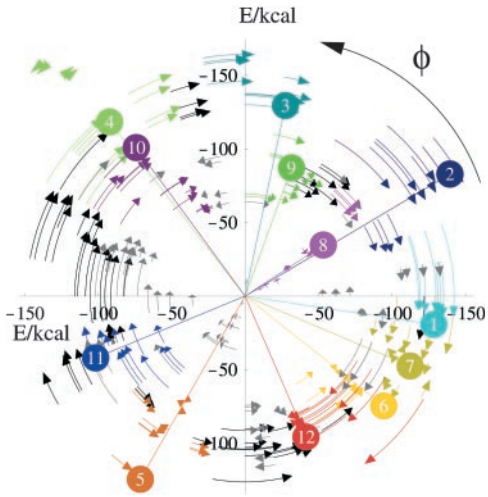

FIG. 3. **Energy of all structures obtained from the global search protocol dependent on the helix rotation parameter ϕ in polar format moving counterclockwise.** The *arcs* represent the energy and ϕ of each final structure, whereas the *arrows* designate the change of ϕ during the simulation from the starting structure. The negative energy is measured as the distance from the origin. Cluster averages are shown as *circles* connected by azimuthal *lines* with the origin.

TABLE II

Parameters of the structures from the global search.

Energy E of each structure, number of structures considered for the average, helix crossing angle Ω, helix rotation parameter ϕ, and rotational pitch angles $\omega_{Gly^{59}/Leu^{66}}$, $\omega_{Gly^{61}/Leu^{68}}$ are given. ω was calculated by geometric analysis of the coordinate file. The angles are averages over all four helices of a structure.

Structure	E/k_{cal}/mol	Number of structures	Ω	ϕ	$\omega_{Gly^{59}/Leu^{66}}$	$\omega_{Gly^{61}/Leu^{68}}$
1	−130	19	16 °	351 °	169 °	6.8 °
2	−162	13	16 °	31 °	224 °	43 °
3	−132	12	14 °	78 °	270 °	86 °
4	−150	15	13 °	128 °	302 °	143 °
5	−133	13	14 °	240 °	53 °	248 °
6	−120	12	16 °	322 °	146 °	321 °
7	−122	15	16 °	337 °	163 °	334 °
8	−64	14	−14 °	33 °	44 °	227 °
9	−93	13	−15 °	70 °	81 °	263 °
10	−125	17	−16 °	126 °	125 °	329 °
11	−110	12	−15 °	202 °	197 °	43 °
12	−104	16	−13 °	293 °	291 °	110 °

from the site-directed dichroism analysis, we have incorporated an orientation refinement energy term in all molecular dynamics and energy minimization calculations as described elsewhere (11). According to the experimental data, a helix tilt restraint was applied. To account for the rotational pitch angle, four site-specific dichroism restraints were applied by setting the angles between the $^{13}C{=}O$ bonds of Gly^{59}, Leu^{66}, Gly^{61}, and Leu^{68} and the z axis to those obtained from the experiment. These angles are a function of the helix tilt β, the rotational pitch angle ω (10). This restraint causes structures that deviate from the experiment to be higher in energy. The rotational pitch angles of the resulting structures were determined from a geometric analysis with a self-written program.

RESULTS AND DISCUSSION

FTIR Measurements—The transmission FTIR spectra of the CM2 peptide reconstituted in lipid vesicles (Fig. 1, *A* and *B*) are indicative of an α-helical structure. FTIR spectroscopy has become a standard tool to determine the secondary structure of proteins (15), and even subtle differences in helical conformations of bacteriorhodopsin have been monitored (22, 23). Quantitative estimates of the secondary structure may be obtained by curve-fitting individual components contributing to the amide I absorption and assigning each component to a certain type

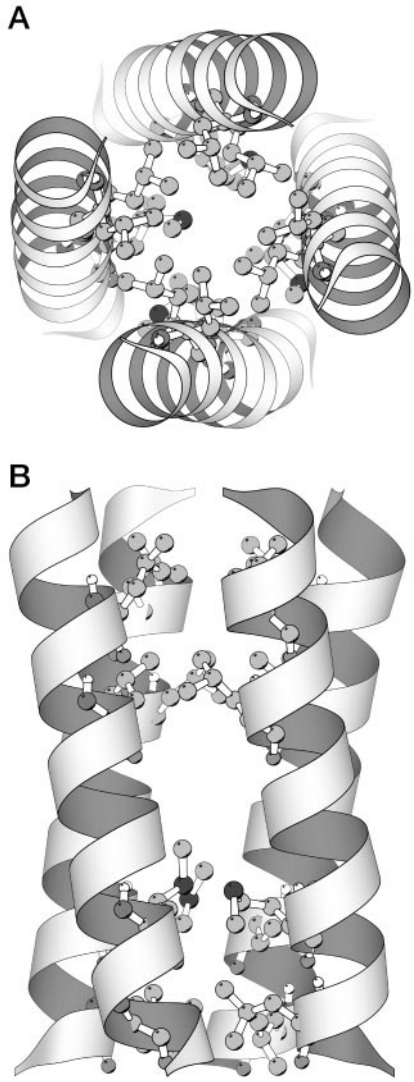

FIG. 4. **Ribbon diagrams of the CM2 transmembrane structure shown from the N terminus from Tyr^{51} to Val^{70} (*top*) and from the side (*bottom*).** The residues pointing into the center, Leu^{55}, Leu^{58}, Met^{65}, and Leu^{68}, are shown in a ball and stick display. The figure was created with MOLSCRIPT (28).

of secondary structure (15). The analysis yields a total of 68% α-helix, 28% unordered, and 3.4% β structure, the latter of which we attribute to not properly reconstituted peptide. This compares well with the 20-residue predicted transmembrane part (2) comprising 69% of the synthesized 29-residue peptide.

To estimate the amount of protein that is not accessible to water and therefore embedded in the membrane, the hydrogen/deuterium exchange was measured using the amide II absorption band (Fig. 1*C*). The amount of exchange after a 4-h incubation in D_2O is 34% of the total amide II absorption. This indicates that the transmembrane part consists of 19–20 residues that are not accessible to water.

The attenuated total reflection-FTIR spectra of the $[^{13}C_1]Gly^{59}/Leu^{66}$- and $[^{13}C_1]Gly^{61}/Leu^{68}$-labeled peptide shown in Fig. 2 are indicative of a perpendicular orientation of the α-helix relative to the membrane plane, because the absorbance obtained with parallel polarized light is more intense than the absorbance obtained with perpendicular polarized light. The dichroic ratios for the helix and the ^{13}C-labeled sites averaged from seven different measurements for each peptide are shown in Table I. The order parameter S, used extensively in conventional infrared dichroism analysis (24), is a measure

FIG. 5. **Slices of the CM2 transmembrane structure.** From top to bottom: Tyr^{51}-Ala^{56}, Ala^{56}-Gly^{61}, Gly^{61}-Leu^{66}, and Leu^{66}-Val^{70}. The figure was created with MOLSCRIPT (28).

of the average orientation of molecules. An order parameter of S = 1 is indicative of an orientation perpendicular to the membrane plane, whereas S = −0.5 indicates an orientation parallel to the membrane plane. The order parameters S calculated for the helix and the lipid bilayer (Table I) are indicative of a well ordered lipid bilayer with helices possessing a net trans-bilayer orientation. The quantitative analysis of the helix and site-specific dichroic ratios yielded a helix tilt angle β = (14.6 ± 3.0)° and a rotational pitch angle $\omega_{Gly^{59}/Leu^{66}}$ = (218 ± 17)° and $\omega_{Gly^{61}/Leu^{68}}$ = (58 ± 17)°. Note that $\omega_{Gly^{61}/Leu^{68}} = \omega_{Gly^{59}/Leu^{66}} + 200°$, as in canonical α-helix (17).

Global Molecular Dynamics Search—A model built using the transmembrane sequence of CM2, YMLTLASLGLGIITMLYLLV, was subjected to a molecular dynamics search protocol assuming a tetrameric symmetrical helix bundle. The molecular dynamics calculations were carried out applying the experimental constraints. The distribution of structures as a function of the energy and the helix rotation parameter ϕ is shown as a polar plot in Fig. 3. The arcs represent the individual structures that are clustered into groups of similar structures. From these clusters average structures were calculated and the energy was minimized. They are shown as numbered circles. The negative energy is given by the distance from the origin. In Fig. 3 and Table II it can be seen that structure number 2 has the lowest energy. Geometric analysis of the structures reveals that structure 2 has a rotational pitch angle ω = 224° (Table II), which is in excellent agreement with the experimental value ω = (218 ± 17)°. It can be seen from the helix crossing angle Ω, that structure 2 forms a left-handed coiled helical bundle. Structure 11, which is right-handed, with ω = 197°, is the next closest to the experimental value but is ruled out not only because of the fact that it is outside the experimental error range, but it also has a much higher energy than the left-handed structure 2. Accordingly, structure 2 was chosen as the correct model for the CM2 transmembrane domain.

Structure Description and Biological Implications—The structure in Fig. 4 reveals a left-handed coiled-coil tetramer where the residues Leu^{55}, Leu^{58}, Met^{65}, and Leu^{68} are pointing toward the pore. The structure is tilted by 15° from the membrane normal. The pore is occluded mainly by Met^{65} and partially by Leu^{55} as it can be seen from the space filling model in Fig. 5. This is in agreement with the data from the deuterium exchange experiments, which revealed that the transmembrane part is not accessible to water. By analogy to the *Influenza* M2 virus proton channel it has been speculated that CM2 has ion channel function as well (2). Based on our structural model, this hypothesis can be supported if we assume a closed conformation of this ion channel with Met^{65} forming part of the gate. The closed conformation is very likely to be present in a partly dehydrated lipid membrane, where it is assumed that the lipids are in a gel phase compared with the more fluid liquid crystalline phase present under *in vivo* conditions. To observe a conformational change to the open conformation, a simulation time in the order of milliseconds would be necessary possibly including the lipid bilayer as well (25), which is not yet feasible with the current speed of computers.

It is interesting to note that the hydrophilic residues Thr^{54}, Ser^{57}, and Thr^{64} are not lining the channel pore but are located at the outer surface. This is in accordance with other ion channel structures forming mostly hydrophobic pores, *e.g.* the K^+ channel (26) or the HIV-I virus vpu protein (18).

The N-terminal extracellular part forms a wide entrance with the first constriction at Leu^{55} (Fig. 5). This entrance could be a possible target for antiviral drugs blocking the channel as it is assumed for amantadine in the *Influenza* M2 virus proton channel (27).

Acknowledgment—We thank Prof. Dennis Pederson and Dr. Jaume Torres for carefully reading the manuscript.

REFERENCES

1. Hongo, S., Sugawara, K., Nishimura, H., Muraki, Y., Kitame, F., and Nakamura, K. (1994) *J. Gen. Virol.* **75,** 3503–3510
2. Pekosz, A., and Lamb, R. A. (1997) *Virology* **237,** 439–451
3. Hongo, S., Sugawara, K., Muraki, Y., Kitame, F., and Nakamura, K. (1997) *J. Virol.* **71,** 2786–2792
4. Duff, K. C., and Ashley, R. H. (1992) *Virology* **190,** 485–489
5. Sunstrom, N. A., Premkumar, L. S., Premkumar, A., Ewart, G., Cox, G. B., and Gage, P. W. (1996) *J. Membr. Biol.* **150,** 127–132
6. Sansom, M. S. P. (1998) *Curr. Opin. Struct. Biol.* **8,** 237–244
7. Sansom, M. S. P., Forrest, L. R., and Bull, R. (1998) *Bioessays* **20,** 1–10
8. Sansom, M. S., Kerr, I. D., Smith, G. R., and Son, H. S. (1997) *Virology* **233,** 163–173
9. Pinto, L. H., Dieckmann, G. R., Gandhi, C. S., Papworth, C. G., Braman, J., Shaughnessy, M. A., Lear, J. D., Lamb, R. A., and DeGrado, W. F. (1997) *Proc. Natl. Acad. Sci. U. S. A.* **94,** 11301–11306
10. Arkin, I. T., MacKenzie, K. R., and Brunger, A. T. (1997) *J. Am. Chem. Soc.* **119,** 8973–8190
11. Kukol, A., Adams, P. D., Rice, L. M., Brunger, A. T., and Arkin, I. T. (1999) *J. Mol. Biol.* **286,** 951–962
12. Kovacs, F. A., and Cross, T. A. (1997) *Biophys. J.* **73,** 2511–2517
13. Kauppinen, J. K., Moffatt, D. J., Mantsch, H. H., and Cameron, D. G. (1982) *Appl. Spectrosc.* **35,** 271–276

14. Tadesse, L., Nazarbaghi, R., and Walters, L. (1991) *J. Am. Chem. Soc.* **113,** 7036–7037
15. Byler, D. M., and Susi, H. (1986) *Biopolymers* **25,** 469–487,
16. Tsuboi, M. (1962) *J. Polym. Sci. Part D Macromol. Rev.* **59,** 139–153
17. Pauling, L., Corey, R. B., and Branson, H. R. (1951) *Proc. Natl. Acad. Sci. U. S. A.* **37,** 205–211
18. Kukol, A., and Arkin, I. T. (1999) *Biophys. J.* **77,** 1594–1601
19. Adams, P. D., Arkin, I. T., Engelman, D. M., and Brunger, A. T. (1995) *Nat. Struct. Biol.* **2,** 154–162
20. Brunger, A. T., Adams, P. D., Clore, G. M., Gros, W. L. P., Grosse-Kunstleve, R. W., Jiang, J. S., Kuszewski, J., Nilges, M., Pannu, N. S., Read, R. J., Rice, L. M., Simonson, T., and Warren, G. L. (1998) *Acta Crystallogr. Sect. D* **54,** 905–921
21. Jorgensen, W., and Tirado-Rives, J. (1988) *J. Am. Chem. Soc.* **110,** 1657–1666
22. Torres, J., Sepulcre, J., and Padros, E. (1995) *Biochemistry* **34,** 16320–16326
23. Cladera, J., Torres, J., and Padros, E. (1996) *Biophys. J.* **70,** 2882–2887
24. Braiman, M. S., and Rothschild, K. J. (1988) *Annu. Rev. Biophys. Biophys. Chem.* **17,** 541–570
25. Tieleman, D. P., Berendsen, H. J. C., and Sansom, M. S. P. (1999) *Biophys. J.* **76,** 1757–1769
26. Doyle, D. A., Cabral, J. M., Pfuetzner, R. A., Kuo, A., Gulbis, J. M., Cohen, S. L., Chait, B. T., and MacKinnon, R. (1998) *Science* **280,** 69–77
27. Lamb, R. A., and Pinto, L. H. (1997) *Virology* **229,** 1–11
28. Kraulis, P. J. (1991) *J. Appl. Crystalogr.* **24,** 946–950